



# Silver Nanostructures for Determination of FKBP12 Protein <sup>†</sup>

Cosimo Bartolini <sup>1</sup>, Martina Tozzetti <sup>1,2</sup>, Stefano Menichetti <sup>1</sup>  and Gabriella Caminati <sup>1,2,\*</sup> 

<sup>1</sup> Department of Chemistry, University of Florence, Via della Lastruccia 3–13, 50019 Sesto Fiorentino, FI, Italy; cosimo.bartolini@unifi.it (C.B.); martina.tozzetti@unifi.it (M.T.); stefano.menichetti@unifi.it (S.M.)

<sup>2</sup> Consorzio Sistemi a Grande Interfase (CSGI), University of Florence, Via della Lastruccia 3, 50019 Sesto Fiorentino, FI, Italy

\* Correspondence: gabriella.caminati@unifi.it

<sup>†</sup> Presented at the 4th International Electronic Conference on Biosensors, 20–22 May 2024; Available online: <https://sciforum.net/event/IECB2024>.

**Abstract:** FKBP12 is a peptidyl—prolyl cis—trans isomerase that was recently proposed as a candidate biomarker for cancer, for neurodegenerations and for anti—rejection therapy after organ transplant. We designed and fabricated a nanosensor platform for the rapid and efficient determination of FKBP12 concentration in biological fluids exploiting anisotropic silver nanoparticles (AgNps) to enhance the capabilities of Quartz Crystal Microbalance (QCM) detection. To this end, the QCM sensor was coated with a compact array of AgNPs that were further functionalized with a Self—Assembled—Monolayer containing a synthetic receptor, GPS—SH1, designed and synthesized specifically to selectively bind FKBP12. Silver nanoflowers, AgNFs, and silver dendrites, AgNDs, were prepared by electrodeposition and characterized by means of UV—Vis spectroscopy, Scanning Electron Microscopy (SEM), QCM and water contact angle (CA). The AgNPs@Au/GPS—SH1—functionalized QCM sensors were used to detect increasing concentrations of FKBP12 in solution; the results showed that the use of AgNDs significantly enhanced the sensitivity of the sensor with respect to flat Ag sensor chips, allowing the detection of FKBP12 at sub—picomolar concentrations.

**Keywords:** FKBP12; nanosensors; silver nanostructures; neurodegenerative diseases; cancer; transplant rejection



**Citation:** Bartolini, C.; Tozzetti, M.; Menichetti, S.; Caminati, G. Silver Nanostructures for Determination of FKBP12 Protein. *Eng. Proc.* **2024**, *73*, 9. <https://doi.org/10.3390/engproc2024073009>

Academic Editor: Michael Thompson

Published: 12 November 2024



**Copyright:** © 2024 by the authors. Licensee MDPI, Basel, Switzerland. This article is an open access article distributed under the terms and conditions of the Creative Commons Attribution (CC BY) license (<https://creativecommons.org/licenses/by/4.0/>).

## 1. Introduction

FKBP12 is a peptidyl—prolyl cis—trans isomerase with a well—established role in cancer, neurodegenerative diseases and anti—rejection response after surgical transplantation [1]; its fast, easy and reliable determination in biological fluids such cerebrospinal fluid (CSF) and blood is therefore essential both in the early diagnosis and treatment of cancer and neurodegenerative pathologies, as well as for efficiently monitoring the correct administration of anti—rejection drugs. The capture and recognition of FKBP12 in solution was achieved using a Self—Assembled Monolayer (SAM) containing the GPS—SH1 receptor, a thiol derivative specifically designed and synthesized to bind the FKBP12 protein, as shown in previous studies [2,3]. GPS—SH1 was used together with different molecular spacers, such as 1—Dodecanethiol (C<sub>12</sub>—SH) and thiol—polyethylene glycol (PEG—SH), to ensure the efficient interaction between the GPS—SH1 receptor and FKBP12 protein by minimizing the interaction between GPS—SH1 molecules and to prevent nonspecific interaction with potential interferents. A schematic representation of the described platform is reported in Figure 1.

The SAM was assembled on a gold or silver coated support for a Quartz Crystal Microbalance (QCM) on which plasmonic silver nanoparticles (AgNPs) were deposited. The synthesis of two types of silver nanostructures, i.e., nanoflowers (AgNFs) and nanodendrites (AgNDs), was investigated with the primary goal of enabling their fabrication using electrodeposition, a technique that allows for obtaining a compact array of silver

nanostructures that directly adhere to the supports, and with the additional aim of creating a hot-spot rich substrate for future Surface-Enhanced Raman Spectroscopy (SERS) applications. We evaluated various methods for the synthesis of AgNPs before selecting electrodeposition; physical methods, such as pyrolysis and spark discharging, allow for rapid synthesis without the use of hazardous chemicals; however, they result in low yield, poor particle uniformity and high energy consumption. On the other hand, chemical synthesis increases the yield and reduces costs but requires reducing agents that are harmful to the environment and living organisms. A viable green alternative is biological synthesis or microwave-assisted synthesis; both methods are eco-friendly and pollutant-free [4]. However, dense and stable coating of the surface with nanoparticles prepared in bulk is not trivial and is in general laborious and time consuming [5]. On the contrary, electrodeposition results in a high yield of tightly packed nanostructures adhering to the substrate, resulting in many SERS-active sites and high specific surface areas.

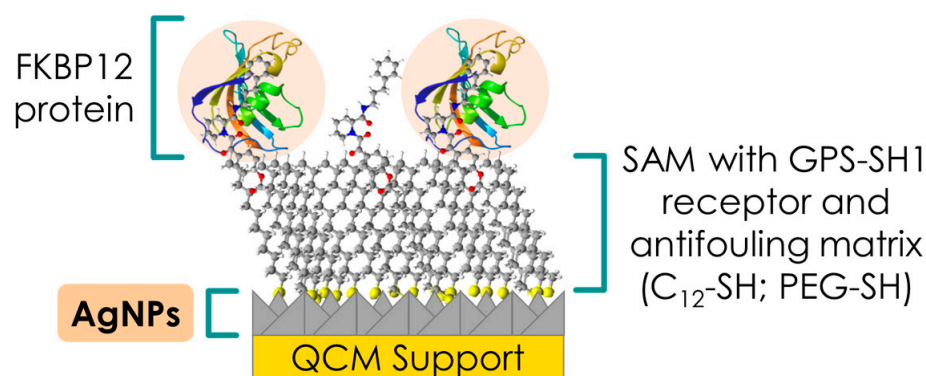


**Figure 1.** Schematic representation of nanosensor for determination of FKBP12.

The present work builds upon a previous patent detailing the *in silico*-design and synthesis of GPS-SH1 [2] and on a recent paper on the development and validation of a nanosensor for FKBP12 in biological fluids [6] using flat gold surfaces.

This study demonstrates that the inclusion of silver nanostructures on the sensor platform enhances the sensitivity for protein detection compared to traditional QCM sensors and provides a basis for implementing other diagnostic techniques such as SERS [7].

## 2. Materials and Methods

FKBP12 (MW 11900) expressed in *E. coli* was supplied by CIRMMP (Florence, Italy). The purity of FKBP12 was greater than 95%, as determined by SDS electrophoresis. The stock concentration ( $C = 2.4009 \times 10^{-5}$  M) of FKBP12 in PBS ( $\text{KH}_2\text{PO}_4/\text{K}_2\text{HPO}_4$  0.5M e NaCl 0.15 M, pH = 7.4) buffer was determined by UV absorbance at 280 nm ( $\epsilon_{280} = 9970 \text{ M}^{-1}$ ) using Nanodrop ONEc Microvolume UV-Vis spectrometer (Thermo Fisher Scientific, Wilmington, DE, USA). GPS-SH1 was synthesized as previously described [2,3].

1-dodecanethiol (C<sub>12</sub>-SH), thiol-polyethylene glycol (PEG-SH), AgNO<sub>3</sub> and KNO<sub>3</sub> were bought from Sigma-Aldrich (Saint Luis, MO, USA) and used without other purifications.

The solutions were prepared using pure water obtained by means of a reverse osmotic system (Milli-RO, Millipore GmbH, Darmstadt, Germany) and by ion exchange and filtration (Milli-Q, Millipore GmbH, Darmstadt, Germany); the resistivity was  $R = 18 \text{ M}\Omega\text{cm}$  and the pH = 5.6.

QCM sensors were bought from Q-Sense (Biolin Scientific AB, Espoo, Finland); the sensors were treated with UV-Ozone cleaner (Boone, IA, USA) for 10 min, then they were submerged in Piranha Basic solution at 70 °C (H<sub>2</sub>O<sub>2</sub> 30% (w/w) in H<sub>2</sub>O mixed with NH<sub>4</sub>Cl at a 1:3 ratio), washed with water, dried with N<sub>2</sub> and treated again with UV-Ozone Cleaner for 10 min.

- Electrodeposition of silver nanostructures

Electrodeposition was conducted at 25 °C using an Autolab PGSTAT30 (Metrohm, Herisau, Switzerland) working station. The electrolyte solution, consisting of AgNO<sub>3</sub> 5 mM and KNO<sub>3</sub> 1 mM, was inserted in an electrolytic cell with three electrodes configuration. An Ag/AgCl reference and platinum counter electrodes were used, while glass/ITO slides or gold QCM support were used as working electrodes.

- UV–Vis spectrophotometer

The absorption spectra of the electrodeposited glass/ITO samples were measured using a Lambda 900 spectrophotometer (Perkin Elmer, Milano, Italy) in the wavelength range 250–860 nm, with a scanning speed of 250 nm/min and a slit width of 1 nm. UV–Vis spectra of FKBP12 in solution were obtained using a Nanodrop ONEc Microvolume UV–Vis spectrophotometer (Thermo Fisher Scientific, Wilmington, DE, USA). Volume 1–2 µL and optical path = 1 cm.

- Scanning Electron Microscopy

SEM micrographs were obtained with a Variable Pressure Hitachi SU3800 SEM equipped with a Ultim Max 40 Analytical Silicon Drift EDS Detector (energy resolution of 127 eV at the Mn–K $\alpha$  line), X4 Pulse Processor and AZtecLive software (Oxford Instruments NanoAnalysis, Abingdon, UK), with an accelerating voltage of 15 kV.

- Contact angle measurements

Contact angle measurements were obtained both by fast screening using a simple home-made setup that consisted of a stand where the samples and a holder were placed to keep the camera aligned parallel to the sample surface and using an Automated Contact Angle Goniometer (Ramé–Hart, Inc., Mountain Lakes, NJ, USA) including a fiber optic light source to reduce water evaporation effects, a CCD camera for image capture and a computer controlled dispenser (Auto Pipetting System, Ramé–Hart, Mountain Lakes, NJ, USA) for drops of controlled volume (2–5 µL). Both right and left contact angles were obtained by image analysis every 5 s until spreading equilibrium was reached. Both methods provided similar results.

- Quartz Crystal Microbalance (QCM)

QCM measurements were performed with a QCM–Z500 (KSV Instruments Ltd., Helsinki, Finland) with impedance monitoring equipped with a thermoelectric (TE) module (Oven Industries, Mechanicsburg, PA, USA) employing a silver- and gold-coated AT-cut 5 MHz quartz crystal (Biolin Scientific, Espoo, Finland) with a frequency stability and resolution of  $\pm 0.05$  Hz in water. The resonant frequency shift ( $\Delta F$ ) was simultaneously measured at the fundamental resonant frequency ( $F_0$ ) and at five odd overtones ( $n = 3, 5, 7, 9, 11$ ), corresponding to resonance frequencies of  $F_n \approx 5, 15, 25, 35, 55$  MHz. The active area of the sensor was 0.785 cm<sup>2</sup>. The measuring cell was kept at  $T = 20.0 \pm 0.1$  °C with a Peltier element connected to the TE module; the room temperature was  $22.0 \pm 0.1$  °C.

The QCM–Z500 response is sensitive to the mass and to the viscoelastic properties of the surface-bound layer. A decrease in  $\Delta F_n$  coupled with low values of  $\Delta D$  and invariance of  $\Delta F_{n/n}$  indicate a rigid film; in this case, the measured frequency shift  $\Delta F$  is linearly proportional to the mass density,  $\Delta m/A$ , of the deposited film according to the Sauerbrey Equation (Equation (1)):

$$\Delta F_n = -\frac{2F_0^2}{A\sqrt{\rho_q\mu_q}}\Delta m \quad (1)$$

where  $n$  is the overtone number and  $\rho_q$  (2.648 g/cm<sup>3</sup>) and  $\mu_q$  (1011 g/cm·s<sup>2</sup>) are the density and the shear modulus of the quartz crystal, respectively [8,9].

### 3. Results and Discussion

#### 3.1. Surface Coating with Anisotropic Silver Nanostructures

Arrays of anisotropic silver nanoparticles (AgNPs) with different morphologies and silver dendritic nanostructures (AgNDs) were obtained from the optimization of the electrodeposition process. Glass/ITO slides of approximately 2 cm<sup>2</sup> were used as substrates. Based on established procedures [10,11], several deposition methods were tested using different compositions of electrolyte solutions, potentials and electrodeposition durations. The samples were characterized through UV–Vis spectroscopy, electron microscopy, and contact angle measurements.

Figure 2A shows anisotropic silver nanoparticles, obtained by applying a potential of  $-0.9$  V for 50 s using an electrolytic solution containing 1 mM AgNO<sub>3</sub>. The sample exhibits a homogeneous surface coverage with AgNPs approximately 70 nm in length and 35 nm in cross-section. It can be observed that individual nanoparticles tend to come close together, forming specific aggregates that resemble flowers. Consequently, these structures have been termed “nano-flowers” (AgNFs). The very close proximity between the individual AgNPs allows the formation of nanogaps of about 10 nm, which serve as interesting hot-spots for achieving significant signal enhancement in SERS [7].

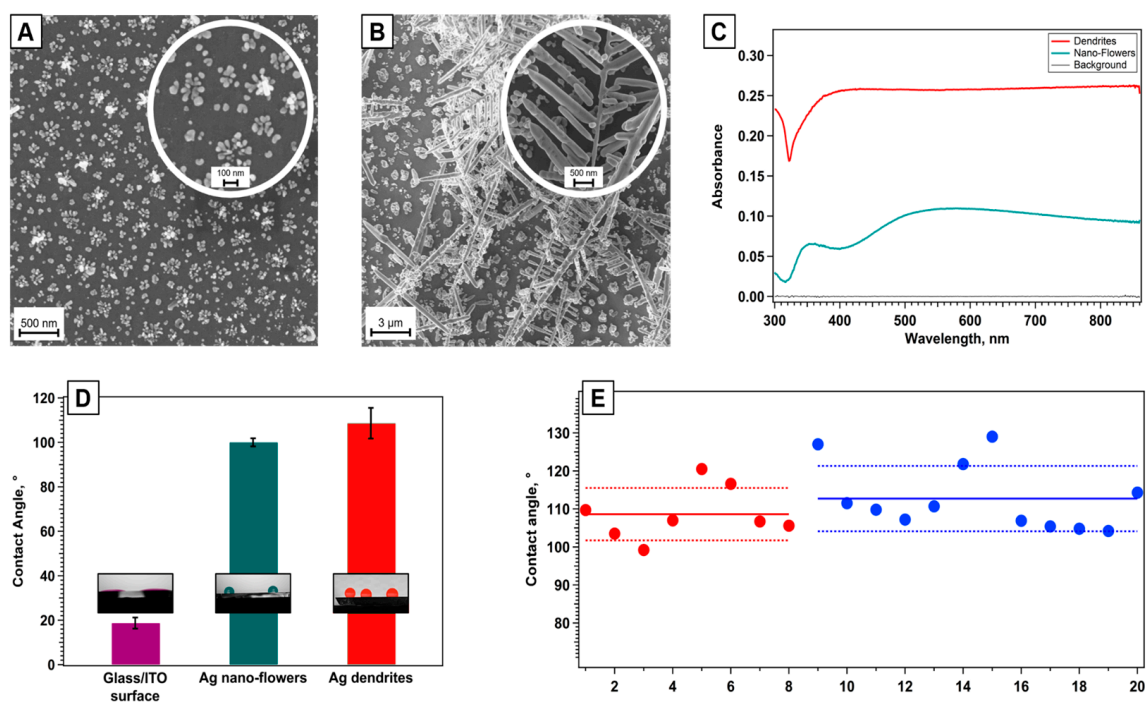


**Figure 2.** (A) SEM image of AgNFs deposited on glass/ITO slides. (B) SEM image of AgNDs deposited on glass/ITO slides. (C) UV–Vis absorption spectra of AgNDs (red) and AgNFs (blue) deposited on glass/ITO slides. (D) Number of 5  $\mu$ L water droplets deposited on UV–Ozone cleaner treated glass/ITO slides (purple), on glass/ITO slides with AgNFs (blue) and on glass/ITO slides with AgNDs (red). Histograms showing average contact angle for three different surfaces. (E) Contact angle measurements for samples with AgNDs: drop volume = 5  $\mu$ L (orange), drop volume = 2  $\mu$ L (blue); solid lines indicates mean value, and dashed lines represent standard deviation.

Figure 2B shows the formation of silver dendritic nanostructures on ITO surface through the application of a potential of  $-0.06$  V for 600 s using an electrolytic solution composed of 5 mM AgNO<sub>3</sub> and 1 mM KNO<sub>3</sub>. Upon macroscopic examination of the sample surface, it is observed that the glass/ITO slide with deposited AgNDs exhibits a lighter coloration, tending towards white. In contrast, the slide with deposited AgNFs exhibits a darker coloration.

The SEM images reveal that, besides AgNDs, there are spherical-like particles present on the sample surface with an average size of 230 nm. This is consistent with the hypothesized growth mechanism for diffusion-limited aggregation (DLA) of AgNDs [12]. For this reason, the surface sample with AgNDs is more heterogeneous than the one with deposited AgNFs. The dendritic structures extend to over a micron in length, while the sharp tips have a cross-section of approximately 30 nm. The high density of these structures and the numerous hot-spots suggest an intense SERS activity.

In Figure 2C, the absorbance spectrum of AgNDs is compared with that of AgNFs. The AgNFs' spectrum shows two broad bands with a first maximum at around 350 nm and another one localized at 540 nm. AgNDs exhibit a very broad signal that extends across the entire visible region and reaches into the infrared. The broad absorption spectrum of AgNDs results from the convolution of multiple bands. As shown in Figure 2B, the trunks and branches are highly variable in size due to the random formation mechanism, resulting in various plasmonic peaks as also supported by the literature [11].

Wettability studies were conducted on the electrodeposited samples by depositing 5  $\mu$ L water droplets in various areas of the sample (Figure 2D), measuring both the contact angles on the right and left sides. The histograms in Figure 2D show the average contact angle for AgNDs and AgNFs compared to the contact angle measured for the ITO surface treated with UV-Ozone cleaner. The mean values measured after the electrodeposition of AgNPs differ significantly from the mean value obtained on glass/ITO slides; the large contact angle values ( $\theta \gg 95^\circ$ ) indicate the presence of superhydrophobic surfaces and confirm the presence of nanostructures. Superhydrophobicity is one of the main characteristics of dendritic nanostructures, leading to very high contact angle values, a behavior well described by the Cassie—Baxter model [13]. We also observed (Figure 2E) that substrates coated with AgNFs exhibit a lower standard deviation compared to samples covered with AgNDs; this finding aligns with SEM observations of good surface uniformity of AgNFs, while the AgND sample appears more heterogeneous.

Surface heterogeneity was also evidenced by the results obtained with different deposited volumes, i.e., 2  $\mu$ L and 5  $\mu$ L. The corresponding CAs are reported in Figure 2E and fall into a range of  $99.2^\circ$  to  $129^\circ$  although with different standard deviations. Larger standard deviations are observed for the measurements obtained depositing 2  $\mu$ L drops, reflecting the larger microheterogeneity of the smaller screened areas.

Wettability study is therefore a very simple characterization method that allows for verification of the successful deposition of silver on the ITO surface. When this technique is complemented with others (such as UV-Vis spectroscopy), it enables discrimination between AgNFs and AgNDs.

Electrodeposition on 5 MHz QCM supports of gold and silver was carried out following the procedures described for deposition on glass/ITO slides. The first procedure involved using a 1 mM  $\text{AgNO}_3$  electrolytic solution with a potential of  $-0.9$  V for 50 s to obtain AgNFs, while the second procedure used a solution of 5 mM  $\text{AgNO}_3$  and 1 mM  $\text{KNO}_3$  with a potential of  $-0.06$  V for 600 s to obtain AgNDs.

The silver mass deposited on each support was calculated by measuring the frequency difference before and after electrodeposition. The quantities of silver deposited on gold and silver QCM supports using the first procedure were 6.3  $\mu$ g and 8.4  $\mu$ g, respectively, whereas using the second procedure, the deposited amounts were 71.9  $\mu$ g and 86.3  $\mu$ g, respectively.

SEM observation revealed that the AgNFs obtained on glass/ITO substrates following the first procedure did not form on the gold and silver QCM supports. Instead, a dense and homogeneous coverage of the surface with asymmetric AgNPs of various shapes was observed. AgNDs were obtained on the QCM supports following the second procedure: the dendrites formed on silver sensor chips were not well structured, while nanostructures with well-developed branches were formed on the gold support. On the gold surface, we observed dendritic structures together with flatter regions covered with spherical AgNPs.

Wettability studies were conducted on gold QCM supports with silver dendrites (AgNDs@Au) following the same methodology used for glass/ITO slides. The results

were consistent with those found for dendrites grown on ITO surfaces, demonstrating the reproducibility of the synthetic procedure.

### 3.2. Formation of SAMs on AgNDs@Au QCM Supports

Formation of SAMs over time was studied using AgNDs@Au QCM supports (Figure 3). The solutions used to assemble the three SAMs were as follows: 1 mM GPS-SH1, 1 mM GPS-SH1/C<sub>12</sub>-SH in a 1:6 ratio and 1 mM GPS-SH1/PEG-SH in a 1:6 ratio. PEG-SH and C<sub>12</sub>-SH were added in specific quantities to GPS-SH1 to simplify protein interaction with the receptor as suggested by a previous study conducted on flat QCM sensors [6,8]. These molecules are chemically inert and do not interact with proteins.

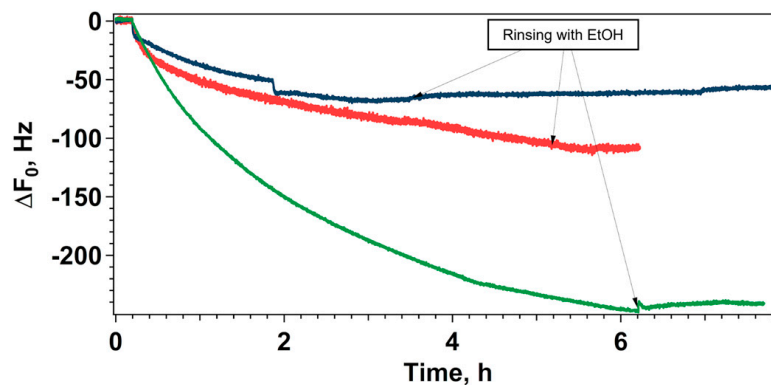


**Figure 3.** Variation in the fundamental frequency during the formation on AgNDs@Au QCM supports of SAMs composed of GPS-SH1 (blue), GPS-SH1/C<sub>12</sub>-SH in a 1:6 ratio (red) and GPS-SH1/PEG-SH in a 1:6 ratio (green).

The adsorbed mass per unit area ( $\Delta m/A$ ) was calculated by the Sauerbrey equation (Equation (1)) from the variation in the fundamental frequency during SAM formation (Figure 3). Experimental data prove that SAMs form a homogeneous monolayer on the surface of AgNDs@Au QCM supports. Table 1 shows that the number of molecules adsorbed on dendrites is significantly higher than those adsorbed on flat QCM supports due to the large surface area exposed by AgNDs. This result is highly promising because a greater quantity of immobilized receptor molecules is expected to enhance the sensitivity of the method for FKBP12, thus lowering the limit of detection (LOD) of the platform.

**Table 1.** Surface density and number of GPS-SH1 molecules per unit area adsorbed on flat gold, flat silver and AgNDs@Au QCM supports.

| QCM Support | SAM Composition                 | $\Delta m/A$<br>(ng/cm <sup>2</sup> ) | Adsorbed GPS-SH1 <sup>a</sup><br>(Molecules/cm <sup>2</sup> ) |
|-------------|---------------------------------|---------------------------------------|---|
| Flat Ag     | GPS-SH1                         | 389                                   | $36.8 \times 10^{13}$   |
| Flat Au     | GPS-SH1                         | 324                                   | $25.7 \times 10^{13}$   |
|             | GPS-SH1/C <sub>12</sub> -SH 1:6 | 136                                   | $4.51 \times 10^{13}$   |
|             | GPS-SH1/PEG-SH 1:6              | 322                                   | $1.54 \times 10^{13}$   |
| AgNDs@Au    | GPS-SH1                         | 1037                                  | $104.9 \times 10^{13}$  |
|             | GPS-SH1/C <sub>12</sub> -SH 1:6 | 1855                                  | $61.8 \times 10^{13}$   |
|             | GPS-SH1/PEG-SH 1:6              | 1699                                  | $8.12 \times 10^{13}$   |

<sup>a</sup> Calculated using the average molecular weight for the 1:6 mixture.

### 3.3. Determination of FKBP12 in Buffer Solution

FKBP12 solutions at different concentrations were added to AgNDs@Au QCM supports functionalized with mixed SAMs of GPS-SH1/C<sub>12</sub>-SH and GPS-SH1/PEG-SH in a 1:6 ratio.

Figure 4 shows the adsorbed mass of FKBP12 per unit area as a function of protein concentration for both platforms. As observed, the data were successfully fitted with the Langmuir model for monolayer adsorption (Equation (2)).

$$\frac{\Delta m}{A} = \frac{\Delta m_{\max}}{A} \cdot \left( \frac{C}{K_d + C} \right) \quad (2)$$

where  $\Delta m/A$  is the measured surface density,  $\Delta m_{\max}/A$  is the saturated surface density,  $C$  is the concentration of FKBP12 in solution and  $K_d$  is the dissociation constant. The  $K_d$  values were calculated from the fitting for the two types of SAMs formed on dendritic silver nanostructures and compared with the values obtained on flat QCM sensors. Additionally, the theoretical saturation surface density ( $\Delta m_{\max}/A$ ) calculated from the fit is compared with the experimentally measured  $\Delta m_{\max}/A$ .

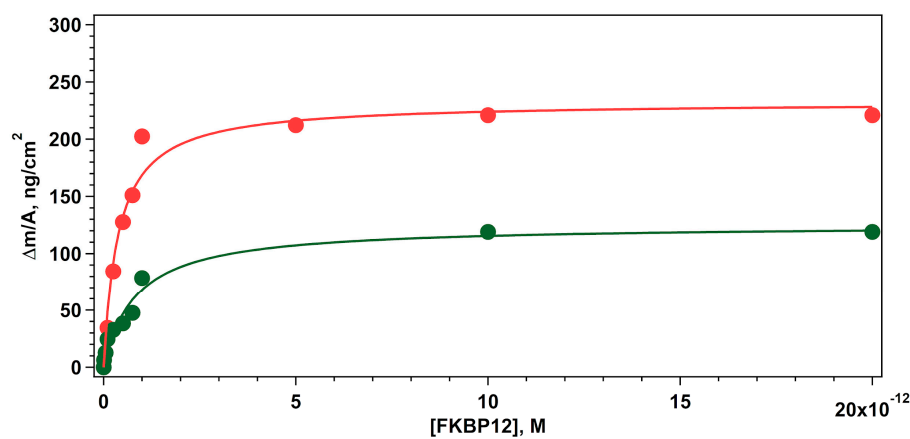


**Figure 4.** Adsorption of FKBP12 as a function of its concentration on SAMs of GPS-SH1/C<sub>12</sub>-SH in a 1:6 ratio (red) and GPS-SH1/PEG-SH in a 1:6 ratio (green) constructed on AgNDs@Au QCM supports.

Table 2 shows the agreement between the theoretical and experimental values of saturation surface density; a strong correlation between these values confirms that the Langmuir model accurately describes the dynamics of the interaction. The data presented in Table 2 reveal that the implementation of silver dendritic nanostructures enables the detection of the protein at lower concentrations compared to the flat sensor.

**Table 2.**  $K_d$  and theoretical  $\Delta m_{\max}/A$  calculated from the fit for flat sensors and sensors with silver dendritic nanostructures and  $\Delta m_{\max}/A$  measured from the experiments.

| QCM Support | SAM Composition                 | $K'_d$ (pM) <sup>b</sup> | $\Delta m_{\max}/A$<br>Theoretical (ng/cm <sup>2</sup> ) | $\Delta m_{\max}/A$<br>Experimental (ng/cm <sup>2</sup> ) |
|-------------|---------------------------------|--------------------------|--|---|
| Flat Au     | GPS-SH1/C <sub>12</sub> -SH 1:6 | 811 ± 169                | 240 ± 2  | 240 ± 7   |
|             | GPS-SH1/PEG-SH 1:6              | 54 ± 12                  | 179 ± 15   | 165 ± 7   |
| AgNDs@Au    | GPS-SH1/C <sub>12</sub> -SH 1:6 | 0.38 ± 0.07              | 232 ± 10   | 221 ± 5   |
|             | GPS-SH1/PEG-SH 1:6              | 0.83 ± 0.13              | 125 ± 5  | 119 ± 1   |

<sup>b</sup> In the case of mixed systems, pseudo- $K'_d$ .

The LOD and the linear range of the sensors were calculated from the linear fitting and the results compared with flat gold sensors are presented in Table 3.

**Table 3.** Saturation mass of FKBP12 adsorbed per unit area on mixed SAMs formed on flat gold and AgNDs@Au QCM supports. Linear range, Limit of Detection (LOD) and R<sup>2</sup> value for linear fit.

| QCM Support | SAM Composition                 | Adsorbed Sat. FKBP12 (Molecules/cm <sup>2</sup> ) | Linear Range (pM) | LOD (pM) | R <sup>2</sup> |
|-------------|---------------------------------|---|-------------------|----------|----------------|
| Flat Au     | GPS-SH1/C <sub>12</sub> -SH 1:6 | $2.58 \times 10^{13}$                             | 4–80              | 8.3      | 0.98576        |
|             | GPS-SH1/PEG-SH 1:6              | $1.41 \times 10^{13}$                             | 4–60              | 6.5      | 0.98592        |
| AgNDs@Au    | GPS-SH1/C <sub>12</sub> -SH 1:6 | $1.08 \times 10^{13}$                             | 2–8               | 0.2      | 0.96398        |
|             | GPS-SH1/PEG-SH 1:6              | $0.58 \times 10^{13}$                             | 0.2–1             | 0.1      | 0.97401        |

The smaller linear range could be attributed to the adsorption on AgNDs with high specific surface area and surface energy, which resulted in a very rapid saturation at low protein concentrations. The R<sup>2</sup> values for the sensors with AgNDs are slightly lower than those obtained for the flat sensor; this may result both from a larger experimental error on bulk concentrations and from the co-presence of a portion of flat gold surface and/or smaller nanostructured surfaces that may hinder an optimal linear fit. In fact, the lower saturation threshold of FKBP12 on the AgNDs@Au platforms also reflects a different absorption behavior that correlates strictly with the different surface energies of the two QCM supports. The flat sensors are characterized by a uniform surface with equivalent surface energy sites, while the AgNDs-covered sensors exhibit regions with different surface energies: the high-energy sites correspond to the tips of dendrites, whereas flat areas and/or small AgNPs are expected to be lower surface energy regions. Therefore, the absorption process on AgNDs@Au supports can be regarded as a multiple steps mechanism and the lower amount of FKBP12 absorbed at saturation may reflect the incomplete covering of all low-energy surface sites. Indeed, preliminary experiments with larger FKBP12 concentrations confirm this hypothesis.

The implementation of AgNDs into the sensor significantly enhances its sensitivity, resulting in an increase in the LOD of at least one order of magnitude compared to flat surfaces. This improvement is primarily attributed to the greater amount of GPS-SH1 adsorbed on the modified sensor. The platform with silver dendrites significantly extends the limit of detection below the picomolar range, seldom observed using QCM detection of proteins [9,14].

Although sub-picomolar LODs have been achieved with ELISA [15] and Tandem LC-MS/MS [16], these studies employ mainly BSA and protein-protein interactions. Few reports are available on FKBP12 detection using LC-MS/MS and ELISA [1]; in this latter case, similar LODs are achieved, but the analytical procedure is more complex, involving multiple steps and requiring several hours of dedicated personnel time. On the other hand, Surface Plasmon Resonance (SPR) provides low LODs, i.e., 0.33 pg/mL for the CD5 protein [17]; the result presented in this work can be directly applied to develop a sensor chip for plasmonic nanostructure-enhanced SPR, which may even further extend the detection limit for FKBP12.

#### 4. Conclusions

Two electrodeposition procedures were successfully developed to obtain AgNFs and AgNDs on glass/ITO slides and QCM gold and silver supports. The characterization of AgNPs using various techniques such as contact angle, UV-Vis spectroscopy, and electron microscopy confirms the formation of AgNFs and AgNDs on ITO/glass substrates and gold- or silver-coated QCM supports. For the development of our detection platform, we selected AgNDs for their superior reproducibility on the different substrates used. SAMs containing the GPS-SH1 receptor and the selected spacer molecules were assembled on AgNDs@Au QCM supports. The results demonstrate that AgNDs@Au QCM supports exhibit a higher quantity of adsorbed receptor molecules compared to flat QCM sensors, enhancing their protein-capture capability. AgNDs@Au sensors were employed for the micro-gravimetric



detection of FKBP12 in solution, showing increased sensitivity compared to traditional QCM sensors for protein detection. Their LOD is indeed comparable to more complex techniques, such as surface plasmon resonance and mass spectrometry, achieving detection of FKBP12 protein at sub-picomolar concentration. Furthermore, the implementation of silver dendritic nanostructures paves the way for the development of a combined QCM-SERS detection device, which could further improve the sensitivity for the determination of FKBP12. This work demonstrates the potential of AgNDs@Au QCM sensors to achieve high sensitivity and reproducibility, positioning them as a powerful tool for protein detection in biological and clinical applications.

**Author Contributions:** Conceptualization, G.C.; methodology C.B., M.T. and G.C.; validation, C.B. and M.T.; investigation, C.B. and M.T.; resources, C.B. and M.T.; data curation, C.B., M.T. and G.C.; writing—original draft preparation, C.B., M.T. and G.C.; writing—review and editing C.B., M.T., G.C. and S.M.; project administration, G.C.; funding acquisition, G.C. and S.M. All authors have read and agreed to the published version of the manuscript.

**Funding:** Funded by the European Union—NextGenerationEU, Mission 4 Component 2, Inv. 1.5—CUP B83C22003920001.

**Institutional Review Board Statement:** Not applicable.

**Informed Consent Statement:** Not applicable.

**Data Availability Statement:** Data are contained within the article.

**Acknowledgments:** Thanks to the MIUR-Italy “Progetto Dipartimenti di Eccellenza 2023–2027” allocated to Department of Chemistry “Ugo Schiff” (Florence), Italy.

**Conflicts of Interest:** The authors declare no conflicts of interest. Views and opinions expressed are however those of the author(s) only and do not necessarily reflect those of the European Union or the European Commission. Neither the European Union nor the European Commission can be held responsible for them. PNRR MUR M4 C2 Inv. 1.5 CUP B83C22003920001.

## References

1. Caminati, G.; Procacci, P. Mounting evidence of FKBP12 implication in neurodegeneration. *Neural Regen. Res.* **2020**, *15*, 2195–2202. [[CrossRef](#)] [[PubMed](#)]
2. Caminati, G.; Procacci, P.; Menichetti, S.; Martina, M.R.; Marsili, L. A Compound for the Determination of the Protein FKBP12 and a Sensor Unit Comprising It. Patent WO 2021/124269 A1, 24 June 2021.
3. Martina, M.R.; Tenori, E.; Bizzarri, M.; Menichetti, S.; Caminati, G.; Procacci, P. The Precise Chemical-Physical Nature of the Pharmacore in FK506 Binding Protein Inhibition: ElteX, a New Class of Nanomolar FKBP12 Ligands. *J. Med. Chem.* **2013**, *56*, 1041–1051. [[CrossRef](#)] [[PubMed](#)]
4. Zhang, X.-F.; Liu, Z.-G.; Shen, W.; Gurunathan, S. Silver Nanoparticles: Synthesis, Characterization, Properties, Applications, and Therapeutic Approaches. *Int. J. Mol. Sci.* **2016**, *17*, 1534. [[CrossRef](#)] [[PubMed](#)]
5. Banchelli, M.; Tiribilli, B.; Pini, R.; Dei, L.; Matteini, P.; Caminati, G. Controlled graphene oxide assembly on silver nanocube monolayers for SERS detection: Dependence on nanocube packing procedure. *Beilstein J. Nanotechnol.* **2016**, *7*, 9–21. [[CrossRef](#)] [[PubMed](#)]
6. Tozzetti, M.; Martina, M.R.; Lucchesi, G.; Vasa, K.; Marsili, L.; Procacci, P.; Menichetti, S.; Caminati, G. Development and validation of a nanostructured sensor for the detection of FKBP12 protein. *ACS Sens.* 2024; submitted.
7. Pilot, R.; Signorini, R.; Durante, C.; Orian, L.; Bhamidipati, M.; Fabris, L. A Review on Surface-Enhanced Raman Scattering. *Biosensors* **2019**, *9*, 57. [[CrossRef](#)] [[PubMed](#)]
8. Höök, F.; Rodahl, M.; Brzezinski, P.; Kasemo, B. Energy Dissipation Kinetics for Protein and Antibody-Antigen Adsorption under Shear Oscillation on a Quartz Crystal Microbalance. *Langmuir* **1998**, *14*, 729–734. [[CrossRef](#)]
9. Tramonti, V.; Lofrumento, C.; Martina, M.R.; Lucchesi, G.; Caminati, G. Graphene Oxide/Silver Nanoparticles Platforms for the Detection and Discrimination of Native and Fibrillar Lysozyme: A Combined QCM and SERS Approach. *Nanomaterials* **2022**, *12*, 600. [[CrossRef](#)] [[PubMed](#)]
10. Hossain, M.K.; Cho, H.Y.; Kim, K.J.; Choi, J.W. Silver Nanostar Patterned Substrate for Label-Free Characterization of Breast Cancer Cells Based on Surface-Enhanced Raman Spectroscopy. *Sci. Adv. Mater.* **2014**, *6*, 2491–2495. [[CrossRef](#)]
11. Sharma, D.K.; Ott, A.; O’Mullane, A.P.; Bhargava, S.K. The facile formation of silver dendritic structures in the absence of surfactants and their electrochemical and SERS properties. *Colloids Surf. A Physicochem. Eng. Asp.* **2011**, *386*, 98–106. [[CrossRef](#)]
12. Mandke, M.V.; Han, S.H.; Pathan, H.M. Growth of Silver Dendritic Nanostructures via Electrochemical Route. *CrystEngComm* **2011**, *14*, 86–89. [[CrossRef](#)]

13. Marmur, A. Soft Contact: Measurement and Interpretation of Contact Angles. *Soft Matter* **2006**, *2*, 12–17. [[CrossRef](#)] [[PubMed](#)]
14. Sudjarwo, W.A.A.; Dobler, M.T.; Lieberzeit, P.A. QCM-based assay designs for human serum albumin. *Anal. Bioanal. Chem.* **2022**, *414*, 731–741. [[CrossRef](#)] [[PubMed](#)]
15. Iha, K.; Inada, M.; Kawada, N.; Nakaishi, K.; Watabe, S.; Tan, Y.H.; Shen, C.; Ke, L.Y.; Yoshimura, T.; Ito, E. Ultrasensitive ELISA Developed for Diagnosis. *Diagnostics* **2019**, *9*, 78. [[CrossRef](#)] [[PubMed](#)]
16. Aebersold, R.; Mann, M. Mass spectrometry-based proteomics. *Nature* **2003**, *422*, 198–207. [[CrossRef](#)] [[PubMed](#)]
17. Fathi, F.; Rashidi, M.H.; Omid, Y. Ultra-sensitive detection by metal nanoparticles-mediated enhanced SPR biosensors. *Talanta* **2019**, *192*, 118–127. [[CrossRef](#)] [[PubMed](#)]

**Disclaimer/Publisher's Note:** The statements, opinions and data contained in all publications are solely those of the individual author(s) and contributor(s) and not of MDPI and/or the editor(s). MDPI and/or the editor(s) disclaim responsibility for any injury to people or property resulting from any ideas, methods, instructions or products referred to in the content.